Journal of Rehabilitation in Civil Engineering 8-4 (2020) 137-155

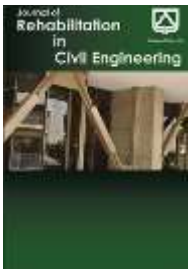

journal homepage: http://civiljournal.semnan.ac.ir/

Improved Seismic Performance of Chevron Brace Frames Using Multi-Pipe Yield Dampers

B. Behzadfar[1], A. Maleki[1*], and M. A. Lotfollahi Yaghin[2]

1. Department of Civil Engineering, Maragheh Branch, Islamic Azad University, Maragheh, Iran
2. Department of Civil Engineering, University of Tabriz, Tabriz, Iran

Corresponding author: A.Maleki@iau-maragheh.ac.ir

ARTICLE INFO

Article history:
Received: 11 February 2020
Accepted: 29 July 2020

Keywords:
Chevron Brace Frames (CBF),
Multi-Pipe Dampers (MPD),
Nonlinear finite element method,
Energy absorption,
Cyclic behavior.

ABSTRACT (Times New Roman 12pt in Bold)

Spacious experimental and numerical investigation has been conducted by researchers to increase the ductility and energy dissipation of concentrically braced frames. One of the most widely used strategies for increasing ductility and energy dissiption, is the use of energy-absorbing systems. In this regard, the cyclic behavior of a chevron bracing frame system equipped with multi-pipe dampers (CBF-MPD) was investigated through finite element method. The purpose of this study was to evaluate and improve the behavior of the chevron brace frame using multi-pipe dampers. Three-dimensional models of the chevron brace frame were developed via nonlinear finite element method using ABAQUS software. Finite element models included the chevron brace frame and the chevron brace frame equipped with multi-pipe dampers. The chevron brace frame model was selected as the base model for comparing and evaluating the effects of multi-tube dampers. Finite element models were then analyzed under cyclic loading and nonlinear static methods. Validation of the results of the finite element method was performed against the test results. In parametric studies, the influence of the diameter parameter to the thickness (D/t) ratio of the pipe dampers was investigated. The results indicated that the shear capacity of the pipe damper has a significant influence on determining the bracing behavior. Also, the results show that the corresponding displacement with the maximum force in the CBF-MPD compared to the CBF, increased by an average of 2.72 equal. Also, the proper choice for the dimensions of the pipe dampers increased the ductility and energy absorption of the chevron brace frame.

DOI: 10.22075/JRCE.2020.19792.1383

1. Introduction

Conventional systems resistant to lateral forces is used in steel structures include concentrically braced frames (CBF), eccentrically braced frames (EBF), steel moment resistant frames (MRF), and steel plate shear walls (SPSWs), and damper-equipped systems. The parameters to be considered in selecting a load-resisting system include stiffness, ductility, capacity, and energy dissipation. Thus, the use of dampers in steel and concrete instruments as an energy-absorption system has increased significantly. In general, energy-absorbing dampers are used to reduce the dynamic response of the structure to seismic loading. Considering the functional mechanism of such devices, through specific deformation and specific mechanical actions, in the seismic loading, they absorb and dissipate large amounts of energy input to the structure [1,2]. One of the methods that have has considered in recent years to retrofit structures is the use of energy-absorbing systems, which provide a desirable reduction in structural displacement [3]. Metallic yielding dampers, as a displacement-correlated type of dampers are the most widely used types of these energy-absorbing systems [4]. Hence, the yielding does not occur on the structural system, but on a predetermined component that can be replaced after loading. The energy dissipation mechanism of all metallic yielding dampers is based on nonlinear deformations of the metallic damper [5–10]. The first research projects on the use of metallic dampers were presented by Kelly and Skinner in the early 1970s [11,12].

The most well-known dampers dissipating input energy to the structure using flexural deformations are Added Damping and Stiffness (ADAS) and Triangular Added Damping and Stiffness (TADAS) [13,14]. The ADAS and TADAS dampers are composed of X-shaped metal plates and triangular plates that dissipate the input energy to the structure by moment deformations. The geometry of these metal plates is designed so that the stress distribution is uniform throughout its height, and all of its parts reach the stage of yielding [15–17]. The slit dampers also utilize the flexural plastic deformation mechanism to dissipate the earthquake input energy, which can to mention numerical and experimental work of Amiri et al. [18], Oh et al. [19] and Chan and Albermani [20]. Hsu and Halim [21,22] presented a special curve-shaped reinforcing element to improve the seismic performance of the structural frame. Palermo et al. [21,22] conducted a numerical and laboratory study to evaluate the performance of the proposed damper. Maleki and Bagheri [23,24] studied the cyclic behavior of pipe dampers in experimental and numerical methods. In this study, the behavior of steel pipes filled with and without concrete was investigated under cyclic shear loading to examine their use as seismic fuses. The results of Maleki and Bagheri's [23] research showed that steel pipes filled without concrete are able to absorb large amounts of energy under intense cycle shear loading with a stable hysteretic behavior. Maleki and Mahjoubi [25–27] dealt with a steel dual-pipe damper and examined it in numerical and experimental methods. The proposed damper system consisted of two welded pipes at selected locations with the loading being applied as a cyclic shear force. Energy was mainly dissipated from cyclic inelastic deformation with the flexural behavior of the pipe. Maleki and Mahjoubi [25–27] observed excellent ductility, energy absorption, and

stable hysteresis rings in all specimens. Also, the finite element models were developed considering nonlinear behavior, large deformation, failure, and damage to materials in order to perform a parametric study on different pipe sizes in this research. Cheraghi and Zahrai [28] presented a concentric dual-tube damper to control concentrically braced frames (CBFs) and to reduce the seismic response of the steel frames. The proposed system consisted of two concentric circular tubes attached to a gusset plate at the brace connection. Cheraghi and Zahrai [28] explored the performance of the proposed damper in an experimental work and through the finite element method. Zahrai and Mortezagholi [29] examined the cyclic performance of elliptical dampers in chevron bracing frames using experimental and numerical methods. The test specimen consisted of two specimens of chevron bracing frames equipped with an elliptical damper. The results revealed good ductility, energy absorption, and stable hysteresis rings in all specimens [23–29]. Studies performed by Abbasnia et al. [30], Bazzaz et al. [31] and Andalib et al. [32] are limited to examining the cyclic behavior and energy absorption of steel ring dampers. Results of studies on SRDs as ductile and energy-absorbing elements in concentrically bracing systems showed good ductility, energy dissipation, and stable hysteresis loops.

The use of multiple pipes as dampers in controlling displacement and increasing ductility as well as the same time significant energy dissipation has attracted the attention of many researchers. In this type of damper system as shown in Fig. 1, a metallic yield damper (multi-pipe yielding dampers) is positioned between the bracket and the upper beam. In multi-pipe dampers with a shear behavior and plastic deformation in low and medium surface earthquakes, it prevents the formation of plastic and buckling in the brace. For the chevron bracing system can be as examples of energy dissipation systems TADAS damper [12,14,15,17], slit dampers [18–20], and shear panels dampers [1,2,6,7] were noted. The energy damping systems provided are suitable for chevron bracing with stable hysteresis behavior and energy absorption but are not cost-effective in construction and interchangeability. Due to the axial behavior of the diagonal brace, the use of a steel ring damper with bending behavior was suggested to improve performance the brace [30]. In chevron bracing systems, the ductile pipe damper is added between the bracing system and the beam to increase the ductility and to prevent damage to the compression member. It also has the capability to be economically installed and replaceable after damage.

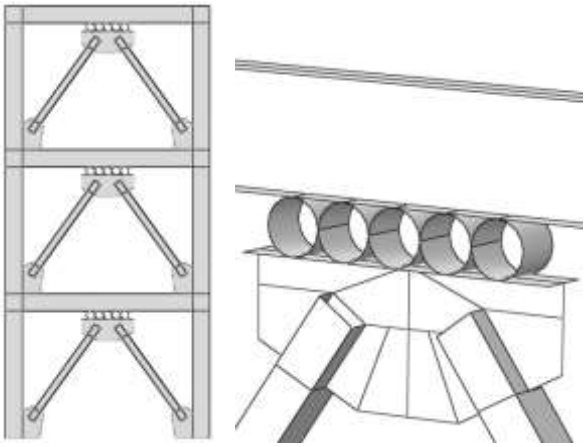

Fig. 1. Chevron bracing frames using Multi-pipe yielding dampers.

Studies performed by Maleki and Bagheri [23,24] and Maleki and Mahjoubi [25–27] are limited to examining the cyclic behavior and energy absorption of pipe dampers. Results of studies on pipe dampers as ductile and energy-absorbing elements in concentrically bracing frame systems showed good ductility, energy dissipation, and stable

hysteresis loops. On the other, these investigations were limited to a few experimental specimens and fixed geometry and details for the pipe dampers. Also, the performance and efficiency of the pipe damper on the concentrically bracing frame systems have not been evaluated by Maleki and Bagheri [23,24] and Maleki and Mahjoubi [25–27]. In this research, parametric studies have been conducted to investigate cyclic behavior of the chevron bracing frame system equipped with a multi-pipe damper.

In this research, multi-pipe dampers presented by Maleki and Mahjoubi [25] are used to be investigated the cyclic behavior of chevron bracing frames. Numerical and experimental investigations of pipe dampers are limited to the dampers, while the damper behavior within the structural system has not been investigated. Thus, it is essential to investigate the cyclic behavior of chevron bracing frame systems equipped with pipe dampers. In this study, is investigated the cyclic behavior of a chevron bracing frame system equipped with a multi-pipe damper. Numerical studies using nonlinear finite element methods and models have been developed using ABAQUS [33] software. Parametric studies included investigating the effect of the diameter to thickness ratio (D/t) of steel pipe on the behavior of a chevron bracing frame system equipped with a multi-pipe damper.

2. Numerical Method

In this study, the numerical method was used to investigate the cyclic behavior of the chevron bracing frame (CBF) system equipped with multi-pipe dampers (MPDs) by the finite element method via ABAQUS [33] software. Following is the introduction of the studied models, the finite element modeling, and validation method.

2.1. The Studied Models

To investigate the cyclic behavior of the chevron bracing frame system as well as the impact of using a multi-pipe damper, the last three floors of a 6-story designed structure, as shown in Fig. 2, was selected. As displayed in Fig. 2, the bay of the CBF is 4.8 m and the same floor height is 3.4 m. The dimensions details of CBF and MPDs are also presented in Table 1. The studied system consists of a dual system CBF and the perimeter gravity frames, where the CBF part resists 100% of the total seismic force [34]. The designs of braces, gusset plates, beams and columns satisfy the requirements of the AISC Seismic Provisions [35]. The cross-sections of the beam and column were made of hot-rolled Iranian IPE and IPB profiles, respectively. The studied models include the CBF and the CBF equipped with a MPD (Fig. 2). The finite element models of the CBF are equipped with a MPD with diameter ratios of 10, 20, 30, and 40 (D/t = 10, 20, 30, and 40).

As revealed in Fig. 2(b), a pipe with a diameter of 200 mm and a length of 180 mm was used. For beam and column sections, IPE400 and IPB400 sections were employed, respectively. Also, hollow section steel (HSS:160×160×5×5) were used for bracing. Plate thickness equal to 10 mm and 2t distance of the bending free line were also considered in the design. The bracing length was 2.75 m and 2.7 m for the CBF equipped without and with MPDs, respectively. For beams, columns, brace, and gusset plate connection, the steel materials St37, and steel pipes from the steel materials St14 were used with a yield stress of 240 MPa and 150MPa,

respectively (Table 1). Also, the elastic properties of steel considered include Poisson's coefficient of 0.3 and modulus of elasticity of 210 GPa. For the entire model, the behavior of the materials is inelastic, and the stress-strain curve is considered as elastic-plastic perfect. The loading was exerted using the cyclic displacement control type and the ATC-24 [36] loading protocol (Fig. 3).

Table 1. Geometric and material property of FE models.

Model	$\frac{D_{Pipe}}{t_{Pipe}}$	Geometric property of models	Yielding stress (MPa)			Pipe thickness (mm)
			Pipe damper	Beam and Column	Brace and Gusset plate	
CBF	-	Gusset plate thickness: 10 mm	-	240	240	-
MPD10	10	Column: IPB400	150	240	240	20
MPD20	20	Beam: IPE400	150	240	240	10
MPD30	30	Brace : □160×160×5×5	150	240	240	6.7
MPD40	40	Pipe damper: ○200×180(D×L)	150	240	240	5.0

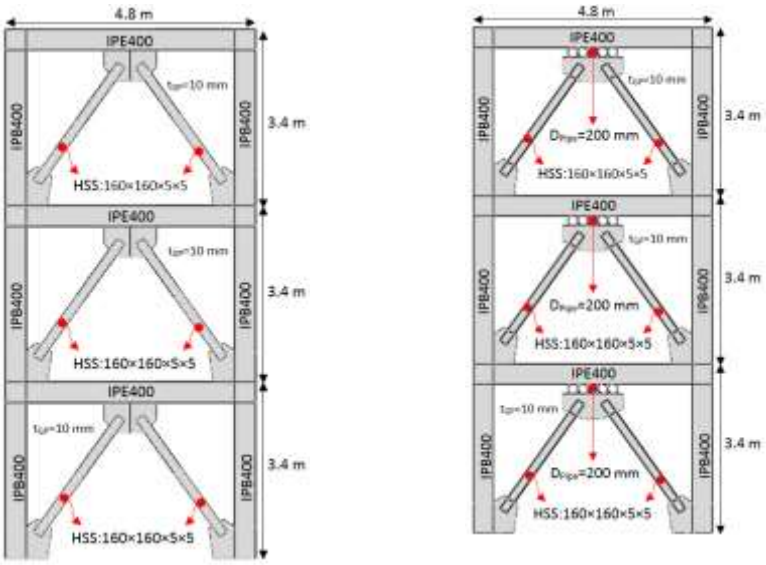

(a) (b)

Fig. 2. Type of FE models studied: (a) Chevron bracing frame, (b) Chevron bracing equipped with multi-pipe damper.

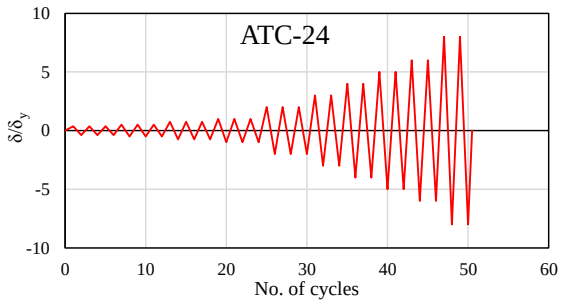

Fig. 3. Loading procedure applied in FE models.

2.2. Nonlinear Finite Element Modeling

This section details the finite element modeling for developing the models selected in the previous section. For the finite element modeling, the models selected in the preceding section of the ABAQUS [33] finite element software are used. The 4-node isotropic shell element (S4R) [33] is employed to model the sections of beams,

columns, braces, pipe dampers, and gusset plates. In the modeling of the nonlinear geometry behavior, the effects of strain hardening, large deformation, and post-buckling behavior are considered for S4R elements. Nonlinear static method [2] (Statics General) and Newton-Raphson method are applied to analyze finite element models.

Material properties modeling was used steel (J2 material properties) for beams, columns, braces, pipe dampers, and gusset plates members [37]. The behavior of the steel material is nonlinear and the stress-strain curve is considered as multi-linear [25]. The plasticity model used is based on the Von-Mises yield surface and the associated flow rule. Plastic strain hardening was considered using nonlinear isotropic and kinematic combine (*COMBINATION HARDENING*). For the elastic area, the modulus of elasticity and Poisson's coefficient were assumed to be 200 GPa and 0.3, respectively. Yield stress used in analyses was taken to be 353 MPa for the CBF model, and 320 MPa for the DPB1L1 and DPB1L2 models according to previous studies, respectively [23,38]. The slope of the strain hardening area is obtained based on the strain stress diagram of Refs. [23,38]. The ultimate tensile strength was taken of 538 MPa for the CBF model in Ref. [38] and 385 MPa for the DPB1L1 and DPB1L2 models in Ref. [23].

Boundary conditions include column supports and lateral support to prevent out-of-plane deformation and cyclic loading. The loading was applied as displacement to the roof level and cyclic, as displayed in Fig. 3. Fig. 4 indicates the boundary conditions and locations of cyclic loading in finite element models. In finite element modeling, due to the absence of imperfections in objects, the initial imperfections in the models must be established. For creating the initial imperfections in the modeling, buckling shape modes are used, where buckling modes are applied to the structure [39]. For this purpose, a buckling analysis was performed, and the first buckling shape mode was used to create the initial imperfection. The initial defect value for the finite element models is assumed to be $L_{br}/1000$, where L_{br} is the bracing length.

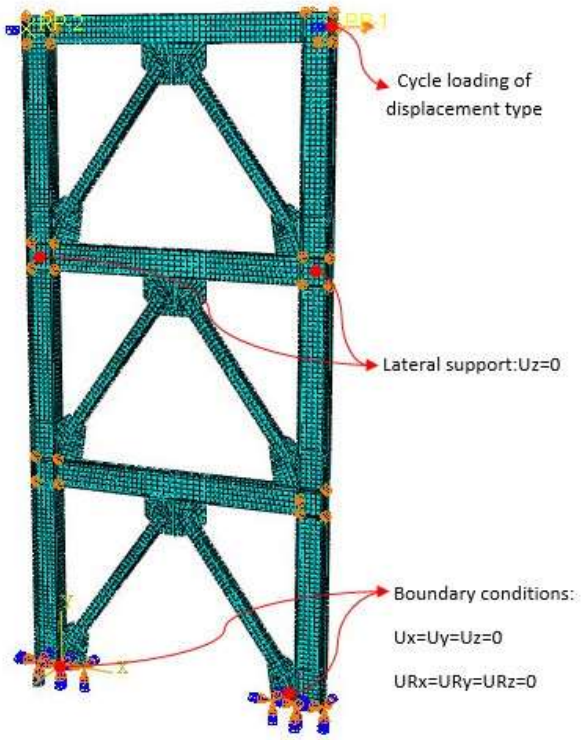

Fig. 4. Loading and boundary conditions in FE models.

2.3. Validation of Finite Element Models

In this part of the research, validation of the results of finite element models with experimental results is investigated. For validation, two samples of pipe dampers tested by Maleki and Bagheri [23] with a chevron brace frame tested by Choi and Park [38] were selected. To evaluate the validity of finite element models, a comparison is made between displacement hysteresis curves and

failure modes with test specimens. Equivalent plastic strain (PEEQ) was used to predict failure areas in finite element models [39].

Maleki and Bagheri [23] pipe dampers were tested at the laboratory of Sharif University. Fig. 5 illustrates the details of the specimen tested by Maleki and Bagheri [23]. As shown in Fig. 5, the experimental specimens consist of two pipe dampers attached to the fixed support on one side and an IPE270 beam on the other. In this study, DPB1L1 and DPB1L2 specimens were used to validate pipe dampers. Fig. 6 reveals the load-displacement hysteresis curve for the DPB1L1 and DPB1L2 specimens tested by Maleki and Bagheri [23] along with the hysteresis curve predicted by the finite element model. The maximum load of the finite element models and experimental results [23] and the error rate of the finite element models are provided in Table 2. The ratio of the maximum shear force predicted by the finite element method to the test specimen is 1.07 and 1.06 for DPB1L1 and DPB1L2, respectively. Fig. 7 illustrates the failure mode of the finite element model and the DPB1L1 experimental specimen. Failure modes include the formation of plastic hinges at the point of attachment to the beam and fixed support. As indicated in Figs. 6 and 7, the predictions of load-displacement hysteresis behavior and finite element model failure modes are consistent with the test results.

Table **2.** Comparison of experimental results and numerical predictions of the maximum load.

Tested by	Specimen	Maximum Laod		Error (%)
		Exp.	FEM	
Maleki and Bagheri [23]	DPB1L1	5.2	5.5	5.7
	DPB1L2	7.8	8.3	6.7
Choi and Park [38]	CBF	1421	1464	1.3
Mean				4.5

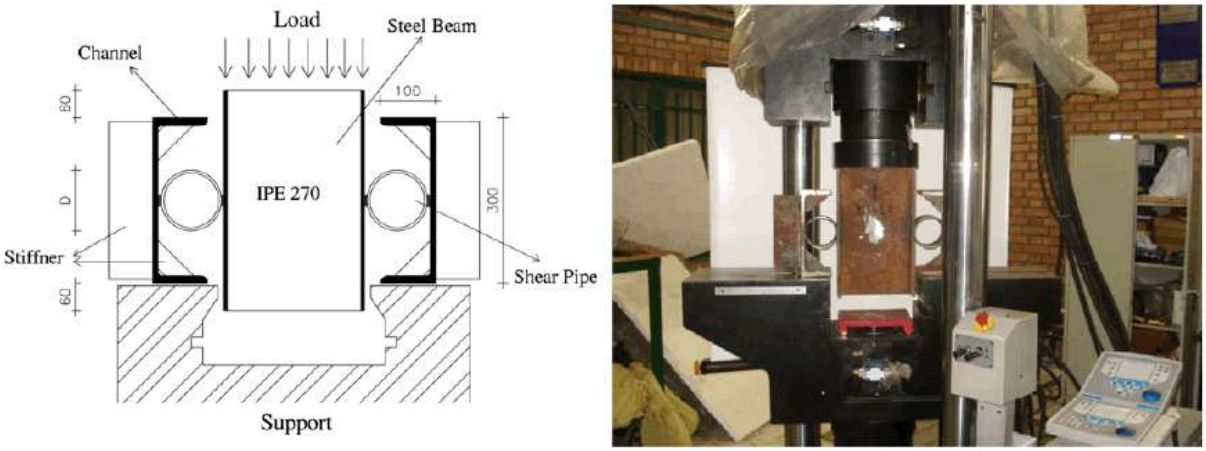

Fig. 5. Details of the sample tested by Maleki and Bagheri [23].

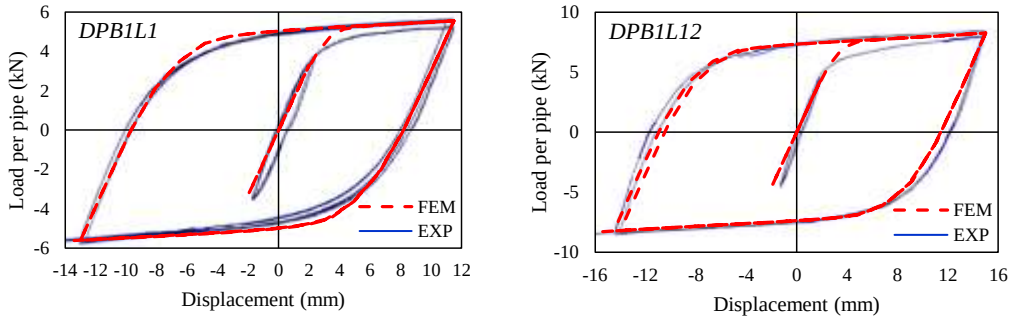

(a) DPB1L1 (b) DPB1L2

Fig. 6. Hysteretic curve comparison of FEM and tested by Maleki and Bagheri [23].

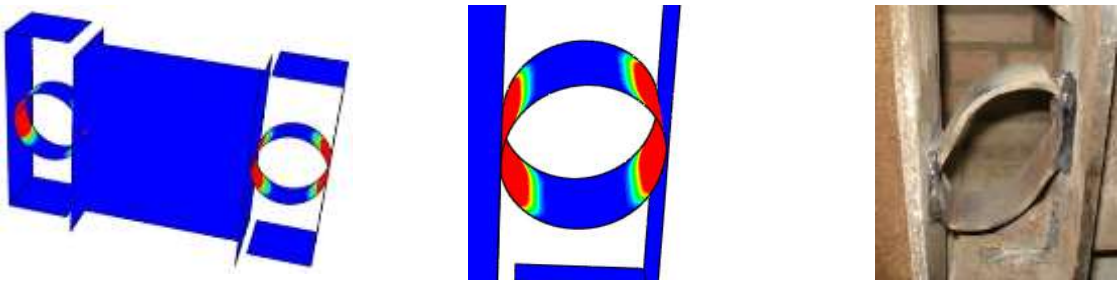

(a) FEM (b) test

Fig. 7. Failure mode comparison of FEM and test specimens of Maleki and Bagheri [23].

Choi and Park [38] tested a 1: 3 scale three-story chevron brace frame (CBF) specimen under cyclic loading. The dimensions and geometries of the CBF specimen tested by Choi and Park [38] are shown in Fig. 8. Fig. 9 reveals the load-displacement hysteresis curve for the CBF sample tested by Choi and Park [38] with the hysteresis curve predicted by the finite element method. The maximum load of the finite element models and experimental results [38] and the error rate of the finite element models are provided in Table 2. The ratio of the maximum shear force predicted by the finite element method to the test specimen is 1.01. Fig. 10 depicts the failure modes of the finite element models and the CBF laboratory specimen. As shown in Fig. 10, the finite element model was able to simulate out-of-plane buckling and the tensile yield on the brace. Comparison of the results of the finite element analysis and the test results reveals good prediction of the cyclic behavior, permanent deformation of the brace, stiffness in the cyclic loading, and failure modes.

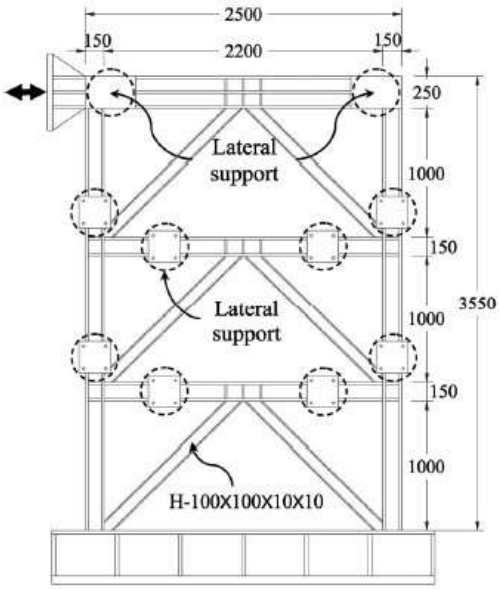

Fig. 8. Details of sample tested by Choi and Park [38].

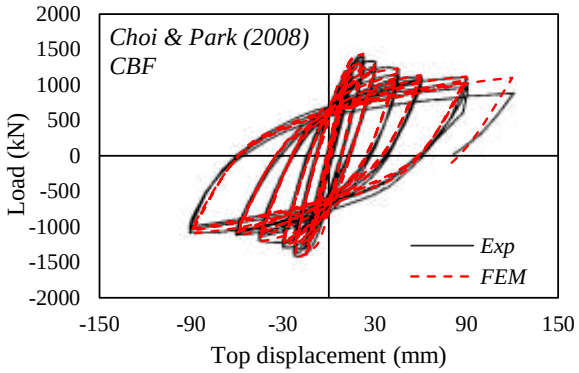

Fig. 9. Hysteretic curve comparison of FEM and tested by Choi and Park [38].

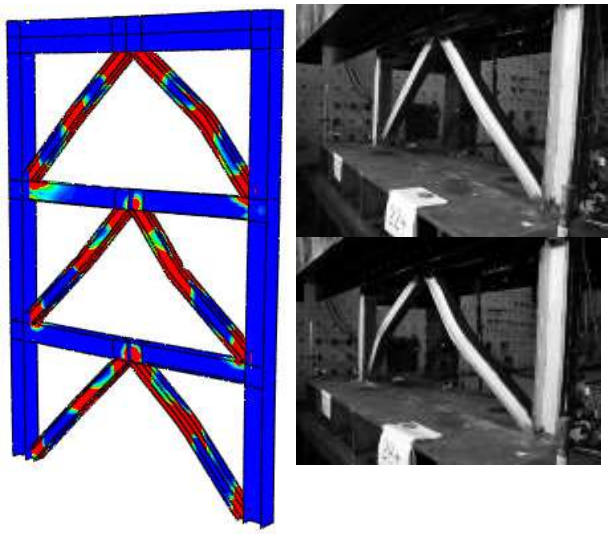

a) FEM (b) test

Fig. 10. Failure mode comparison of FEM and test specimens of Choi and Park [38].

3. Results of Finite Element Models

The finite element models of the chevron brace frame and the chevron brace frame equipped with the multi-pipe dampers provided in geometric details in Table 1 have been quasi-static analyzed according to the ATC-24 [36] cyclic loading protocol. The results of finite element models include hysteresis curves, lateral stiffness, and energy dissipation, which are presented in this section further.

3.1. Model CBF

The finite element model of CBF consists of a steel frame with a chevron brace. This model has been selected as the base model to compare the effects of pipe dampers on bracing system behavior. The CBF model was analyzed under the ATC-24 [36] cyclic loading protocol by a nonlinear static method. The load-displacement hysteresis diagram obtained for the CBF model is shown in Fig. 11. According to the hysteresis curve, the maximum base shear is 1187 kN, which occurred at a 0.74% drift ratio. Equivalent plastic strain was used to investigate the failure mode in the finite element model CBF. Fig. 12 displays the equivalent plastic strain distribution for the CBF model. The failure modes are also depicted based on the drift ratio shown in the hysteresis curve in Fig. 11. The location of the maximum base shear event is shown by point A in Fig. 11. According to Fig. 12(a) at point A, the failure modes are the yields in the tensile braces and the buckling initiation in the compression braces.

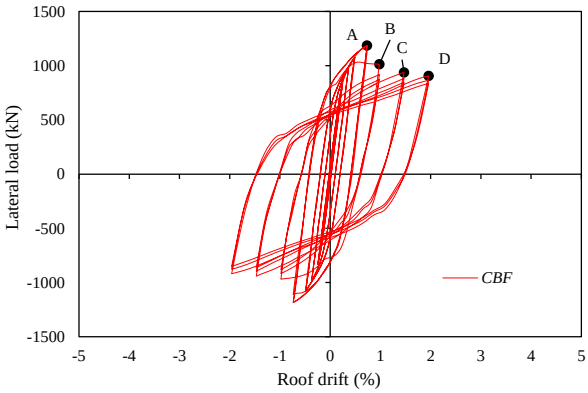

Fig. 11. Hysteretic lateral load–roof drift ratio for models CBF.

Also, the greatest extent of failure distribution is observed in the second-floor braces. According to Fig. 12b, with an increase in floor drift by up to 1%, which is

equivalent to point B, the development of tensile and out-of-plane buckling is observed in braces. At 1.47% drift, equivalent to point C, Fig. 12(c) shows the formation of plastic hinges in the beams and permanent deformation for bracing. At point D, a more significant drop in resistance is observed for local buckling at the webs of the beam, along with the formation of plastic hinges and permanent buckling and plastic hinges formation at the foot of the column (Fig. 12(d)).

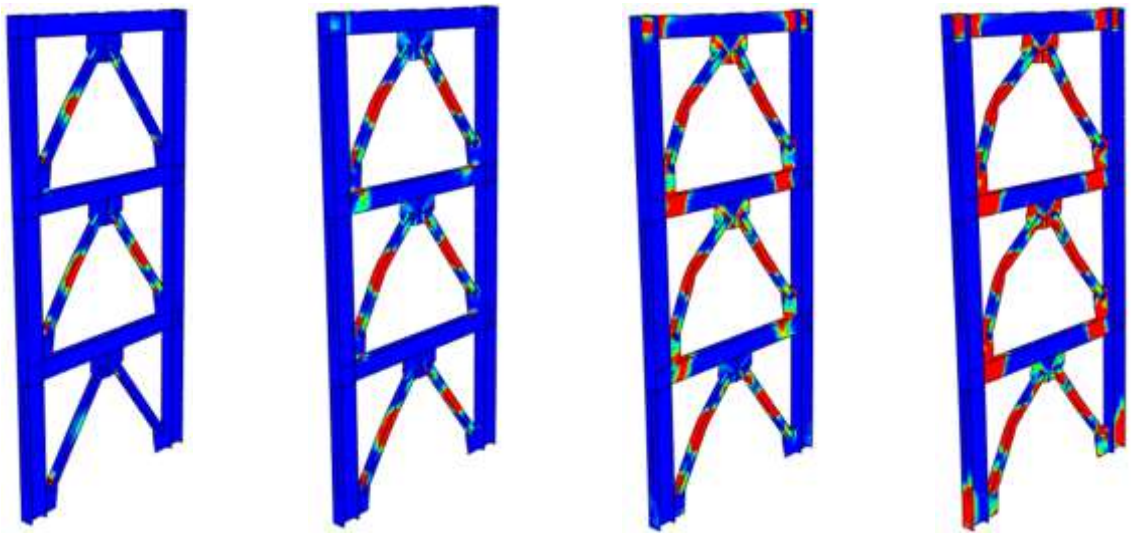

(a) Point A (b) Point B (c) Point C (d) Point D

Fig. 12. Failure mode for models CBF.

3.2. Model MPD10

The MPD10 finite element model includes a chevron brace frame equipped with the multi-pipe dampers with five pipes 200 mm in diameter, 180 mm long, and 20 mm thick. In this model, the diameter-to-thickness ratio of pipes is 10. The load-displacement hysteresis diagram obtained for the MPD10 model is displayed in Fig. 13. According to the hysteresis curve, the maximum base shear is 924 kN, which occurred at a 0.74% drift ratio. The failure modes of model MPD10 are also revealed based on the drift ratio shown in the hysteresis curve in Fig. 13. The location of the maximum base shear event by point B is shown in Fig. 13. According to Fig. 14(a), at point A, the failure modes was observed by the yielding of the pipe dampers in the shear force and the yield of restricted areas of the brace near the gusset plate connection. According to Fig. 14(b), with an increase in the floor drift by 0.74% which is equivalent to point B and as the maximum base shear occurred, the yield pipe of dampers as well as tensile yields and buckling are observed in the braces. Also, limited yields are observed on the upper flange and webs of the second and third-floor beams. At 1.47% drift, equivalent to point C, Fig. 14(c) depicts the formation of plastic hinges in the beams and permanent deformation for bracing. At point D, a more significant fall in resistance is observed for local buckling at the webs of the beam, along with the formation of plastic hinges and

permanent buckling and plastic hinges formation at the foot of the column (Fig. 14(d)). The reason for the reduced capacity in this model may be due to the high shear capacity of the pipe damper to the brace buckling capacity, causing the braces buckling to reach maximum capacity pipe damper before reaching.

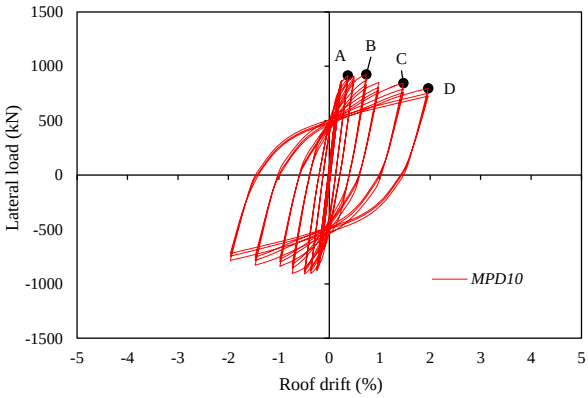

Fig. 13. Hysteretic lateral load–roof drift ratio for models MPD10.

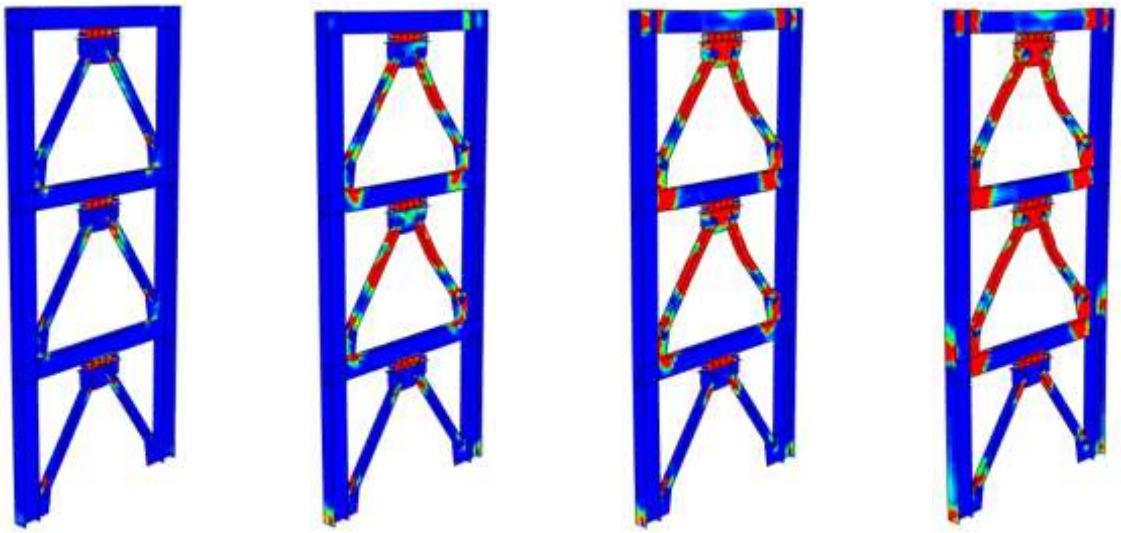

(a) Point A (b) Point B (c) Point C (d) Point D

Fig. 14. Failure mode for models MPD10.

3.3. Model MPD20

The MPD20 finite element model includes a chevron brace frame equipped with the multi-pipe dampers with five pipes 200 mm in diameter, 180 mm long, and 10 mm thick. In this model, the diameter-to-thickness ratio of pipes is 20. The load-displacement hysteresis diagram obtained for the MDP20 model is revealed in Fig. 15. According to the hysteresis curve, the maximum base shear is 1033 kN, which occurred at a 2.94% drift ratio. Fig. 16 indicates the equivalent plastic strain distribution for the MPD20 model. The failure modes of model MPD20 are also shown based on the drift ratio shown in the hysteresis curve in Fig. 15. The location of the maximum base shear event by point C is shown in Fig. 15. According to Fig. 16(a), at point A the failure modes are governed by the yielding of the pipe dampers in the shear force. According to Fig. 16(b), with the increase in floor drift by 1.47%, which is equivalent to point B, the yield of pipe dampers and formation of plastic hinges are observed in the beams. According to Fig. 16(c), at 2.94% drift ration equivalent to the

point C where the maximum base shear occurred, plastic hinges formed in the beams and the brace yielding, the yielding of the outer flanges and webs columns, and the pipe damper. At point D, the formation of plastic hinges in the beams, local buckling on the beam flange, and the formation of plastic hinges at the foot of the column are observed (Fig. 16(d)). Also, at point D, the base cut value is 1026 which is a less reduction in capacity due to the formation of local buckling in the beams and columns.

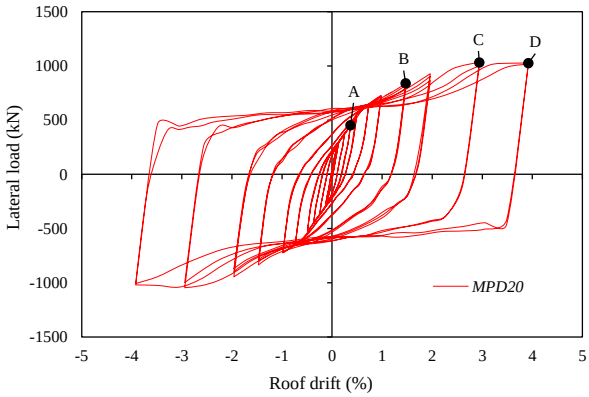

Fig. 15. Hysteretic lateral load–roof drift ratio for models MPD20.

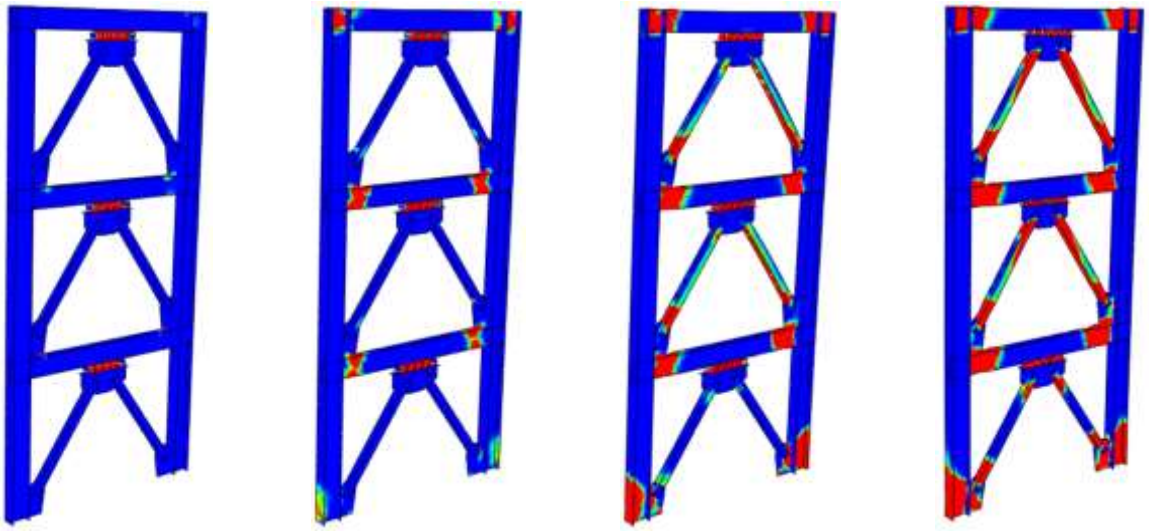

(a) Point A (b) Point B (c) Point C (d) Point D

Fig. 16. Failure mode for models MPD20.

3.4. Model MPD30

The MPD30 finite element model includes a chevron brace frame equipped with the multi-pipe dampers with five pipes 200 mm in diameter, 180 mm long, and 6.7 mm thick. In this model, the diameter-to-thickness ratio of pipes is 30. The load-displacement hysteresis diagram obtained for the MPD30 model is demonstrated in Fig. 17. According to the hysteresis curve, the maximum base shear is 971 kN, which occurred at a 2.94% drift ratio. Fig. 18 shows the equivalent plastic strain distribution for the MPD30 model. The failure modes of model MPD30 are also revealed based on the drift ratio shown in the hysteresis curve in Fig. 17. The location of the maximum base shear event by point C is shown in Fig. 17. According to Fig.18(a) at point A, the failure modes are observed by the pipe damper yields of 0.37% drift ratio. According to Fig. 18(b), with the increase in floor drift by 0.98%, which is equivalent to point B, the yield of pipe dampers and formation of plastic hinges are observed in the beams. According to Fig.

18(c) at 2.94% drift ration equivalent to the point C where the maximum base shear occurred, plastic hinges formed in the beams and the brace yielding, the yielding of the outer flanges and webs columns, and the pipe damper. At point D, the formation of plastic hinges in the beams, local buckling on the beam flange, and the formation of plastic hinges at the foot of the column are observed (Fig. 18(d)).

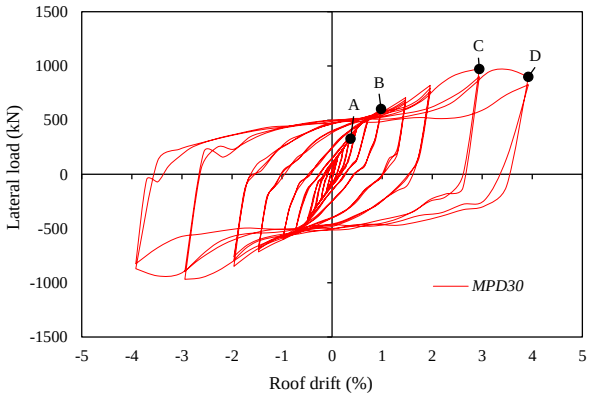

Fig. 17. Hysteretic lateral load–roof drift ratio for models MPD30.

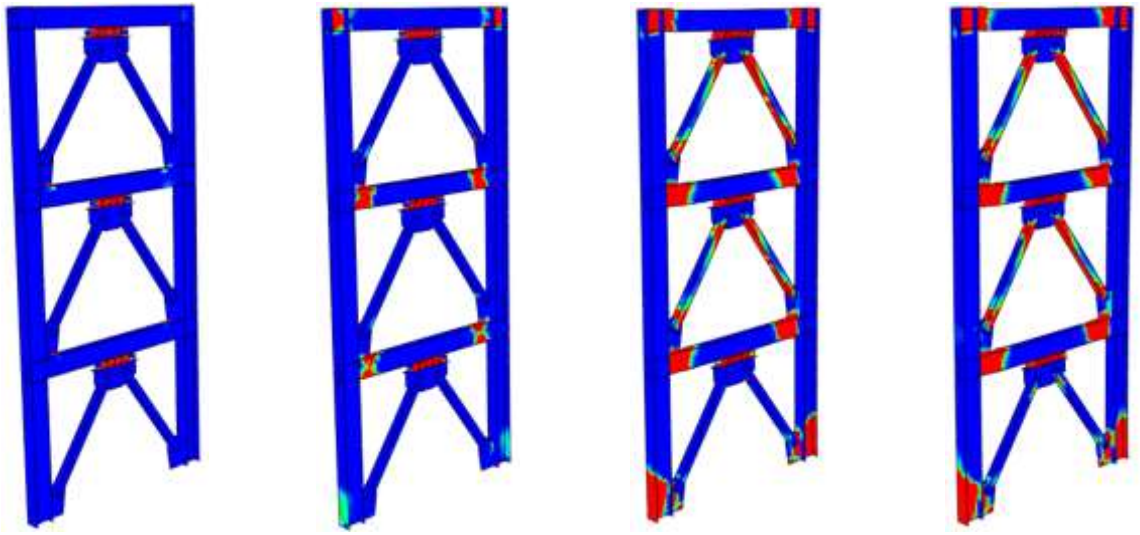

(a) Point A (b) Point B (c) Point C (d) Point D

Fig. 18. Failure mode for models MPD30.

3.5. Model MPD40

The MPD40 finite element model includes a chevron brace frame equipped with the multi-pipe dampers with five pipes 200 mm in diameter, 180 mm long, and 5 mm thick. In this model, the diameter-to-thickness ratio of pipes is 40. The load-displacement hysteresis diagram obtained for the MPD40 model is indicated in Fig. 19. According to the hysteresis curve, the maximum base shear is 824 kN, which occurred at a 2.40% drift ratio. Fig. 20 shows the equivalent plastic strain distribution for the MPD40 model. The failure modes of model MPD40 are also illustrated based on the drift ratio shown in the hysteresis curve in Fig. 19. The location of the maximum base shear event by point C is shown in Fig. 19. According to Fig. 20(a) at point A, the failure modes are observed by the pipe damper yields of 0.37% drift ratio. According to Fig. 20(b), with the increase in the floor drift by 0.98%, which is equivalent to point B, the pipe dampers the yield where plastic hinges formation are observed in the beams. According to Fig. 20(c), at 2.40% drift ration equivalent to the point C where

the maximum base shear occurred, plastic hinges formed in the beams and the brace yielding, the yielding of the outer flanges and webs columns, and the pipe damper. At point D, the formation of plastic hinges in the beams, local buckling on the beam flange, and the formation of plastic hinges at the foot of the column are also observed (Fig. 20(d)).

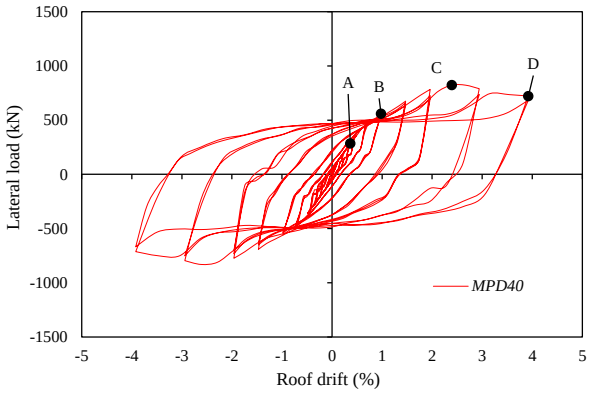

Fig. 19. Hysteretic lateral load–roof drift ratio for models MPD40.

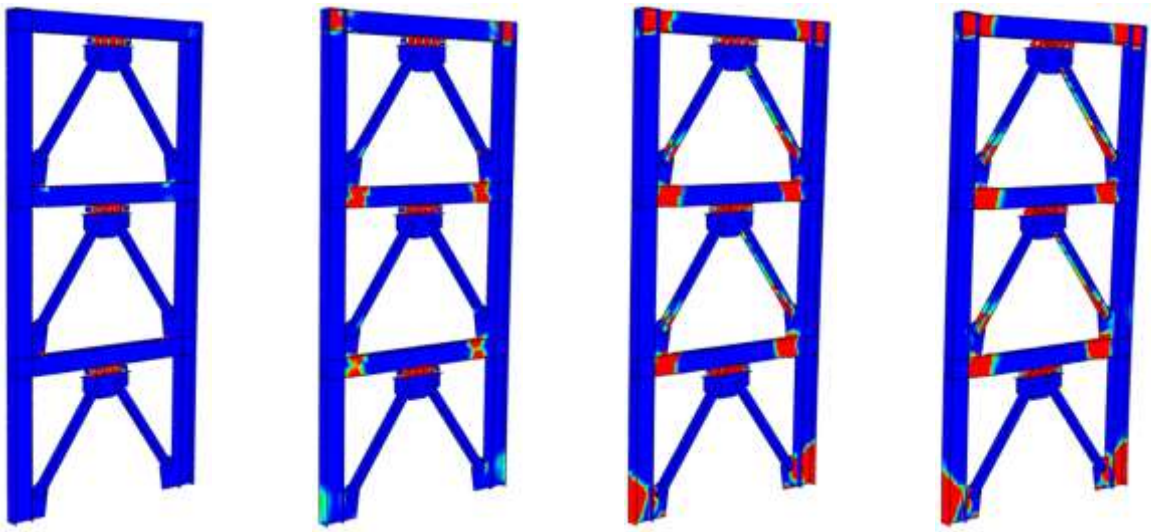

(a) Point A (b) Point B (c) Point C (d) Point D

Fig. 20. Failure mode for models MPD40.

4. Comparison and Effect of Multi-Pipe Dampers on the Behavior of CBF

4.1. General Behavior

In order to compare the general behavior of finite element models, the envelope curve of all hysteresis curves is shown in Fig. 21. Using of pipe dampers has reduced the stiffness and capacity of the chevron bracing frame system. The reduction in stiffness of the CBF system is due to the lower shear stiffness of the pipe damper than the axial stiffness of the braces. Also, upon the shrinkage of the thickness of the pipe dampers, the base shear capacity was also reduced. In the MPD10 model, it behaves similar to the CBF model in that it occurs before the usage of the full shear capacity of the dampers in the buckling braces (Fig. 14). This may be due to the high shear capacity of the pipe dampers relative to the buckling brace capacity. This capacity relativity caused brace buckling before reaching the maximum ductility of the pipe dampers. The buckling occurrence in compression is also shown for the CBF model both in the PEEQ

distribution contours of Fig. 12 and in the load-roof drift diagram of Fig. 21. In many building codes [40–43], floor drift is used as a damage parameter or performance levels of the structure. The FEMA 356 [43] guidelines describe performance levels based on floor drift according to Table 3. In Fig. 21 shows the limited performance level based on FEMA 356 [43] guidelines and according to Table 3 for parametric models. According to Fig. 21 in both models CBF and MPD40, with the was occurred of buckling in the bracing, the desired performance levels are not achieved. However, in models MPD10, MPD20 and MPD30, with the occurrence of the desired mechanism, the yielding of the pipe damper, the formation of plastic hinges in the beams and the columns, the models have reached the performance levels immediate occupancy (IO), life safety (LS) and collapse prevention (CP), respectively.

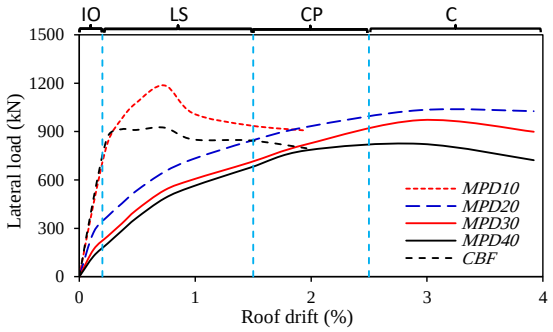

Fig. 21. Envelope curves and performance levels for FE models.

Table 3. Performance levels, type of damage and drift corresponding to performance levels [43].

Performance levels	Type of Damage	Drift
Immediate Occupancy (IO)	No damage	0.0≤
Life Safety (LS)	Moderate repairable damege	0.2≤
Collapse Prevention (CP)	Several damege	1.5≤
Collapse (C)	Collapse damage	≥2.5

4.2. Stiffness

Fig. 22 reveals the variations of the stiffness reduction of the finite element models to the drift ratio of the roof. Stiffness secant in each cycle was used to plot the variation curves of the stiffness reduction. The stiffness secant of each cycle is the slope of the line between the origin and the peak point of the cycle. As can be seen in Fig. 22, the stiffness reduction rates are almost the same across all specimens. In all finite element models, the elastic behavior region exhibited a roof drift ratio of 0.125%. The highest initial rigidity belonged to the CBF model with a value of 39 kN/mm. Among the models equipped with pipe dampers, the highest stiffness at 36 kN/mm was found for the MPD10 model. In the MPD10 model, due to the combination of shear and axial stiffness at the start of loading, it presented high stiffness compared to other models equipped with pipe dampers. In models equipped with pipe dampers, the initial stiffness of the models diminished with thickness reduction. The initial stiffness of the MPD30, MPD20, and MPD40 models was 22, 13, and 10 kN/mm, respectively. As shown in Fig. 22, the stiffness reduction of the two CBF and MPD10 models was at 2% roof drift ratio to equal the stiffness of the other models. This large decline in stiffness is due to the capacity loss due to buckling brace.

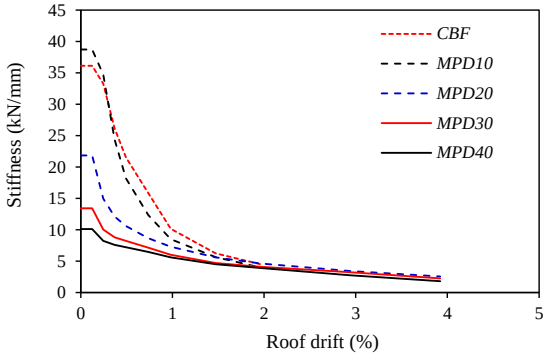

Fig. 22. Stiffness degradation for FE models.

4.3. Energy Dissipation

To compare the extent of energy dissipation by finite element models under cyclic loading, the confined surface inside the obtained hysteresis loops was used. For this purpose, the energy dissipation of the finite element models was computed with the cumulative values of energy dissipation to drift ratio displayed in Fig. 23. According to the hysteresis shapes and loops of the finite element models, it was observed that the MPD20 model depreciates more energy than the CBF and MPD10 finite element models. The reason for this behavior in the MPD20 model as compared to the CBF and MPD10 models is the transfer of the correct force to the fuse and the yielding of the pipe dampers before buckling or tensile brace. The MPD30 and MPD40 models hadalso greater energy absorption and dissipation than the CBF and MPD10 models due to the S-shape and stable loops.

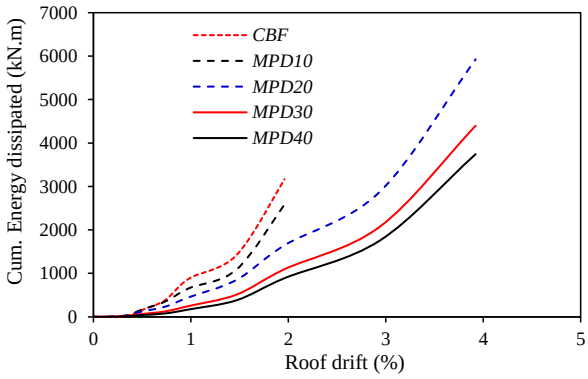

Fig. 23. Cumulative energy dissipation for FE models.

5. Conclusions

Studies performed on the pipe dampers are limited to examining the cyclic behavior and energy absorption. Results of studies on pipe dampers as ductile and energy-absorbing elements in concentrically bracing frame systems showed good ductility, energy dissipation, and stable hysteresis loops. On the other, these investigations were limited to a few experimental specimens and fixed geometry and details for the pipe dampers. Also, the performance and efficiency of the pipe damper on the concentrically bracing frame systems have not been evaluated. In this research, parametric studies have been conducted to investigate cyclic behavior of the chevron bracing frame system equipped with a multi-pipe damper. The cyclic behavior of the chevron bracing frame with pipe dampers was investigated numerical method. Nonlinear finite element models, the chevron bracing frame, and the chevron bracing frame system equipped with multi-pipe dampers were developed for numerical studies. Finite element models under cyclic loading were analyzed by a nonlinear static method. These models were validated against experimental results. In finite element modeling, geometrical nonlinear behavior of materials was considered. In parametric studies, the influence of the diameter parameter to the thickness (D/t) ratio of the pipe dampers was investigated. The results of numerical studies included load-displacement hysteresis curve, elastic hardness, ultimate capacity, and total energy dissipation. The results revealed that the shear capacity of the pipe damper has a significant influence on the determination of bracing behavior. According to the results of parametric studies, the optimal design and performance of model MPD10 have a high ductility, energy dissiotion and ultimate capacity. Also, the results show that the corresponding displacement with the maximum force in the CBF-MPD compared to the CBF, increased by an average of 2.72 equal. Also, the proper choice for the dimensions of the pipe dampers enhances the ductility and energy absorption of the chevron brace frame.

REFERENCES

[1] Zhang C, Aoki T, Zhang Q, Wu M. Experimental investigation on the low-yield-strength steel shear panel damper under different loading. J Constr Steel Res 2013;84:105–13. https://doi.org/10.1016/J.JCSR.2013.01.014.

[2] Chen Z, Dai Z, Huang Y, Bian G. Numerical simulation of large deformation in shear panel dampers using smoothed particle hydrodynamics. Eng Struct 2013;48:245–54. https://doi.org/10.1016/J.ENGSTRUCT.2012.09.008.

[3] Kheyroddin A, Gholhaki M, Pachideh G. Seismic evaluation of reinforced concrete moment frames retrofitted with steel braces using IDA and Pushover methods in the near-fault field. J Rehabil Civ Eng 2018;0:1–15. https://doi.org/10.22075/jrce.2018.12347.1211.

[4] Mohammadi M, Kafi MA, Kheyroddin A, Ronagh HR. Experimental and numerical investigation of an innovative buckling-restrained fuse under cyclic loading. Structures 2019;22:186–99. https://doi.org/10.1016/j.istruc.2019.07.014.

[5] Rai DC, Annam PK, Pradhan T. Seismic testing of steel braced frames with aluminum shear yielding dampers. Eng Struct 2013;46:737–47. https://doi.org/10.1016/J.ENGSTRUCT.2012.08.027.

[6] Zhang C, Zhang Z, Shi J. Development of high deformation capacity low yield strength steel shear panel damper. J Constr Steel Res 2012;75:116–30. https://doi.org/10.1016/J.JCSR.2012.03.014.

[7] Xu L-Y, Nie X, Fan J-S. Cyclic behaviour of low-yield-point steel shear panel dampers. Eng Struct 2016;126:391–404. https://doi.org/10.1016/J.ENGSTRUCT.2016.08.002.

[8] Sahoo DR, Singhal T, Taraithia SS, Saini A. Cyclic behavior of shear-and-flexural yielding metallic dampers. J Constr Steel Res 2015;114:247–57. https://doi.org/10.1016/J.JCSR.2015.08.006.

[9] Hsu H-L, Halim H. Brace performance with steel curved dampers and amplified deformation mechanisms. Eng Struct 2018;175:628–44. https://doi.org/10.1016/J.ENGSTRUCT.2018.08.052.

[10] Qu B, Dai C, Qiu J, Hou H, Qiu C. Testing of seismic dampers with replaceable U-shaped steel plates. Eng Struct 2019;179:625–39. https://doi.org/10.1016/J.ENGSTRUCT.2018.11.016.

[11] Kelly JM, Skinner RI, Heine AJ. Mechanisms of energy absorption in special devices for use in earthquake resistant structures. Bull NZ Soc Earthq Eng 1972;5:63–88.

[12] Skinner RI, Kelly JM, Heine AJ. Hysteretic dampers for earthquake-resistant structures. Earthq Eng Struct Dyn 1974;3:287–96. https://doi.org/10.1002/eqe.4290030307.

[13] Bergman D. Evaluation of cyclic testing of steel-plate devices for added damping and stiffness. Ann Arbor Mich.: Dept. of Civil Engineering University of Michigan; 1987.

[14] Whittaker AS, Bertero V V., Thompson CL, Alonso LJ. Seismic Testing of Steel Plate Energy Dissipation Devices. Earthq Spectra 1991;7:563–604. https://doi.org/10.1193/1.1585644.

[15] Tsai K, Chen H, Hong C, Su Y. Design of Steel Triangular Plate Energy Absorbers for Seismic-Resistant Construction. Earthq Spectra 1993;9:505–28. https://doi.org/10.1193/1.1585727.

[16] Yeh CH, Lu LY, Chung LL, Huang CS. Test of a Full-Scale Steel Frame with TADAS. Earthq Eng Eng Seismol 2001;3.

[17] Gray MG, Christopoulos C, Packer JA. Cast Steel Yielding Brace System for Concentrically Braced Frames: Concept Development and Experimental

Validations. J Struct Eng 2014;140:04013095. https://doi.org/10.1061/(ASCE)ST.1943-541X.0000910.

[18] Ahmadie Amiri H, Najafabadi EP, Estekanchi HE. Experimental and analytical study of Block Slit Damper. J Constr Steel Res 2018;141:167–78. https://doi.org/10.1016/j.jcsr.2017.11.006.

[19] Oh SH, Kim YJ, Ryu HS. Seismic performance of steel structures with slit dampers. Eng Struct 2009;31:1997–2008. https://doi.org/10.1016/j.engstruct.2009.03.003.

[20] Chan RWK, Albermani F. Experimental study of steel slit damper for passive energy dissipation. Eng Struct 2008;30:1058–66. https://doi.org/10.1016/J.ENGSTRUCT.2007.07.005.

[21] Hsu HL, Halim H. Improving seismic performance of framed structures with steel curved dampers. Eng Struct 2017;130:99–111. https://doi.org/10.1016/j.engstruct.2016.09.063.

[22] Hsu HL, Halim H. Brace performance with steel curved dampers and amplified deformation mechanisms. Eng Struct 2018;175:628–44. https://doi.org/10.1016/j.engstruct.2018.08.052.

[23] Maleki S, Bagheri S. Pipe damper, Part I: Experimental and analytical study. J Constr Steel Res 2010;66:1088–95. https://doi.org/10.1016/j.jcsr.2010.03.010.

[24] Maleki S, Bagheri S. Pipe damper, Part II: Application to bridges. J Constr Steel Res 2010;66:1096–106. https://doi.org/10.1016/j.jcsr.2010.03.011.

[25] Maleki S, Mahjoubi S. Dual-pipe damper. J Constr Steel Res 2013;85:81–91. https://doi.org/10.1016/j.jcsr.2013.03.004.

[26] Maleki S, Mahjoubi S. Infilled-pipe damper. J Constr Steel Res 2014;98:45–58. https://doi.org/10.1016/j.jcsr.2014.02.015.

[27] Mahjoubi S, Maleki S. Seismic performance evaluation and design of steel structures equipped with dual-pipe dampers. J Constr Steel Res 2016;122:25–39. https://doi.org/10.1016/J.JCSR.2016.01.023.

[28] Cheraghi A, Zahrai SM. Innovative multi-level control with concentric pipes along brace to reduce seismic response of steel frames. J Constr Steel Res 2016;127:120–35. https://doi.org/10.1016/J.JCSR.2016.07.024.

[29] Zahrai SM, Hosein Mortezagholi M. Cyclic Performance of an Elliptical-Shaped Damper with Shear Diaphragms in Chevron Braced Steel Frames. J Earthq Eng 2018;22:1209–32. https://doi.org/10.1080/13632469.2016.1277436.

[30] Abbasnia R, Vetr MGH, Ahmadi R, Kafi MA. Experimental and analytical investigation on the steel ring ductility. J Sharif Sci Technol 2008;52:41–8.

[31] Bazzaz M, Andalib Z, Kheyroddin A, Kafi MA. Numerical comparison of the seismic performance of steel rings in off-centre bracing system and diagonal bracing system. Steel Compos Struct 2015;19:917–37. https://doi.org/10.12989/scs.2015.19.4.917.

[32] Andalib Z, Kafi MA, Kheyroddin A, Bazzaz M. Experimental investigation of the ductility and performance of steel rings constructed from plates. J Constr Steel Res 2014;103:77–88. https://doi.org/10.1016/j.jcsr.2014.07.016.

[33] ABAQUS-6.8-1. standard user's manual. Hibbitt, Karlsson and Sorensen, Inc. vols. 1, and 3. Version 6.8-1. USA: 2008.

[34] IS2800. Iranian Code of Practice for Seismic Resistant Design of Buildings, Standard No. 2800. Tehran, Iran: 2014.

[35] AISC 341-16. AISC Committee, Seismic Provisions for Structural Steel Buildings. America: 2016.

[36] ATC-24. Guidelines for cyclic seismic testing of components of steel structures. California: 1992.

[37] Mohebkhah A, Azandariani MG. Shear resistance of retrofitted castellated link beams: Numerical and limit analysis approaches. Eng Struct 2020;203:109864. https://doi.org/10.1016/j.engstruct.2019.109864.

[38] Choi I-R, Park H-G. Ductility and Energy Dissipation Capacity of Shear-Dominated Steel Plate Walls. J Struct Eng 2008;134:1495–507. https://doi.org/10.1061/(ASCE)0733-9445(2008)134:9(1495).

[39] Gorji Azandariani M, Gholhaki M, Kafi MA. Experimental and numerical investigation of low-yield-strength (LYS) steel plate shear walls under cyclic loading. Eng Struct 2020;203. https://doi.org/10.1016/j.engstruct.2019.109866.

[40] Vision2000 S. Performance-based seismic engineering. Structural Engineers Association of California, Sacramento, CA: 1995.

[41] ATC-40. Seismic evaluation and retrofit of concrete buildings. 1996.

[42] FEMA 273-274. Federal Emergency Management Agency, NEHRP Guidelines and Commentary for the Seismic Rehabilitation of Buildings. Washington, DC.: n.d.

[43] FEMA 356. Federal Emergency Management Agency, Prestandard and Commentary for the Seismic Rehabilitation of Buildings. Washington, DC, USA: 2000.